

Changes in the Phase-Structure State of Pd–In–Ru Alloy Foils after Hydrogenation and Prolonged Relaxation

V. M. Avdyukhina, O. V. Akimova, I. S. Levin, and G. P. Revkevich

Department of Physics, Moscow State University, Moscow, 119991 Russia

e-mail: vmaphys@gmail.com, olga_vla@bk.ru, is.levin@physics.msu.ru

Received February 24, 2014; in final form, March 31, 2014

Abstract—The structural X-ray analysis of the phase-structure state of the Pd–In–Ru alloy foil after two types of hydrogenation and relaxation (during 8200 h) was carried out. The broadening of the distribution function of the coherent scattering regions (CSRs) with respect to the concentration of indium atoms in the alloy matrix was found to be independent of the foil hydrogenation. The differences in the phase-separation processes on the opposite sides of and the orientation dependencies in the additional phase enriched by vacancies or indium atoms were revealed.

Keywords: hydrogen, X-ray diffraction, palladium-based alloys, evolution of the defect structure, phase transformations.

DOI: 10.3103/S0027134914040031

1. INTRODUCTION

The interest in metal-hydrogen (Me–H) systems covers a wide range of problems from purely scientific to strictly applied ones. These systems are nonequilibrium and open, and their behavior is not described by laws of equilibrium thermodynamics [1]. In such systems, the deviation from the equilibrium state is provided by hydrogen, which enters the crystal lattice under a rather high pressure. Hydrogen migration under saturation and degassing, fluctuations in the composition of the matrix alloy, and differences in specific volumes of coexisting phases induce the origination and transformation processes in such systems during the relaxation of the defect structures, whose nontrivial character was described in [2, 3]. As of now, because of the incompleteness of the theory, the character and degree of changes in the structural state of the Me–H systems after the exposure to hydrogen cannot be predicted. Therefore, the studies of the structural evolution of alloys, its duration, character, and dependence on the initial system state and hydrogenation conditions, are rather topical.

From the practical viewpoint, due to the need to replace fossil energy sources with hydrogen fuel, active projects to enhancing the technology for obtaining high-purity hydrogen from different compounds are being carried out, as no pure hydrogen is available in nature. One of the most environmentally-friendly methods of obtaining hydrogen is the separation of industrial dump gas mixtures with the use of hydrogen-permeable membranes as filters. As palladium and palladium-based alloys are distinguished for their

extremely high sorptive capacity and selective transmission capacity with respect to hydrogen, they are widely used as diffusion filters to obtain high-purity hydrogen [4, 5]. In [5], the high corrosion resistance and hydrogen-permeability of Pd–5.3 at % In–0.5 at % Ru alloy foils, whose characteristics outperform those of the Pd–Ag and B₁ alloys that are now being used in industry to obtain hydrogen, were discussed. The change in the structural state of the foils during relaxation (up to 500 h) after hydration was studied in [6, 7]. However, the nonmonotonic evolution of the structural characteristics in the palladium-based alloys is known to last for tens of thousands of hours, even when there is almost no hydrogen in the system [1, 2]. First of all, this is due to the nonmonotonic redistribution of component atoms in the alloy matrix. This process is rather rapid due to that fact that a great number of vacancies enter the system during hydration [8], which favors a considerable increase of the diffusion coefficient of alloy components.

The nonmonotonic structural evolution can considerably precipitate the hydrogen degradation in hydrogenous materials. Therefore, the study of the evolution is topical both from the fundamental viewpoint and for the development of principles for improving the safety of using hydrogenous materials.

This work is dedicated to studying the phase-structure state of a Pd–In–Ru–H alloy foil after a prolonged (8200 h) relaxation.

2. SAMPLES AND METHOD FOR PROCESSING OF EXPERIMENTAL RESULTS

A Pd–5.3 at % In–0.5 at % Ru alloy foil (50 μm in thickness) was obtained at the Institute of Metallurgy and Material Science of the Russian Academy of Sciences using electric arc alloying and cold rolling of workpieces with intermediate vacuum annealing [4]. Two samples were fabricated using source-annealed foil. One of the samples was exposed to a hydrogen flux while being used as a filter in an device for determining the hydrogen permeability of foils. The hydrogenation was performed at 300°C. The same sample was then electrolytically saturated with hydrogen (the electrolyte was a 4% NaF water solution) during 0.5 h at a current density of 10 mA/cm². After both the hydrogenations, the sample was kept at room temperature for 1 year. The second sample was used as a reference (reference sample).

The diffraction pattern was studied from both sides of the foil using X-ray diffractometry with Bragg–Brentano focusing and CuK $_{\alpha 1}$ -radiation. For the sake of brevity, the side where hydrogen entered the foil is referred to as the saturation side (the A side), while the opposite side is referred to as the B side.

When analyzing diffraction peaks, the Fityk-0.9.4 and Origin-7.5 software packages were used, which are suitable even for a complex shape of diffraction curves.

Taking the low concentration of Ru atoms in the studied alloy (0.5 at %) into account and the fact that the atomic radii of palladium and ruthenium differ by less than 2%, the phase diagrams of the Pd–In and Pd–In–H systems [9] were used to interpret the experimental data, since there are no state diagrams for the Pd–In–Ru and Pd–In–Ru–H systems in the literature.

In this work, the shape, normalized intensity, and the expansion of diffraction curve were studied [6, 7]. The physical broadening of the diffraction peak is determined as follows:

$$\beta_{h/2} = B_{h/2} - b_{h/2}, \quad (1)$$

where $b_{h/2}$ is the instrumental broadening of the diffraction curve of the reference at half-height and $B_{h/2}$ is the width of the studied diffraction curve at half-height [10].

The diffractograms of the 111, 200, 220, 311, 222, and 400 lines were obtained. For the control sample, these correspond to the symmetrical curves described by one Gaussian function with an almost identical width, which is regarded as the instrumental broadening of the diffraction curve ($b_{h/2} = 0.100^\circ$). From the A side, the lattice spacing is $a = (3.9077 \pm 0.0004) \text{ \AA}$, which corresponds, according to the Vegard dependence [11], to the indium-atom concentration $C_{\text{In}} = (5.3 \pm 0.1) \text{ at \%}$; from the B side, $a = (3.9070 \pm 0.0004) \text{ \AA}$ and $C_{\text{In}} = (5.1 \pm 0.1) \text{ at \%}$. Thus, in the initial state, the

indium-atom concentration for both sides differed by 0.2 at %.

The nondimensional quantity $\frac{\Delta a}{a}$, which was determined from the physical broadening of the peaks, is a characteristic of the distribution function of the coherent scattering regions (CSRs) with respect to the concentration of In atoms in the sample [12]:

$$\beta_{h/2} = 2 \frac{\Delta a}{a} \tan(\theta), \quad (2)$$

since one can turn from Δa (using the Vegard dependence) to ΔC_{In} .

In order to determine the effect of a small degree of dispersion of the sample (CSR size along the normal to the surface of the sample (D)) and magnitude of microdeformations (ε) on the diffraction peak smearing in the case where the diffraction curve is described by a Gaussian function, the following expression is used [12]:

$$\beta^2 = \left(\frac{\lambda}{D \cos \theta} \right)^2 + 16 \varepsilon^2 \tan^2 \theta. \quad (3)$$

With β , D , and ε being positive, we can write the following for two orders of reflection:

$$\begin{aligned} & (\beta \cos \theta)_{2h2k2l}^2 - (\beta \cos \theta)_{hkl}^2 \\ & = \varepsilon^2 (\tan^2 \theta_{2h2k2l} - \tan^2 \theta_{hkl}). \end{aligned} \quad (4)$$

Then, we have the following:

$$(\beta \cos \theta)_{2h2k2l}^2 > (\beta \cos \theta)_{hkl}^2 \frac{\cos^2 \theta_{hkl}}{\cos^2 \theta_{2h2k2l}}. \quad (5)$$

If, when analyzing the experimental data, inequality (5) does not hold, then the effect of the small degree of dispersion and presence of microdeformations in the sample studied on the widening of diffraction curves cannot be determined, since it will be determined by the fact that there is a set of lattice spacings in the sample, i.e., the distribution of the CSR with respect to the concentration of alloy-component atoms is not a δ -function. Note that the analysis of the diffraction lines 111 and 200 characterizes the state of the near-surface layer (from 0 to 3 μm for the X-ray wavelength used) of the alloy, while the analysis of the 220, 222, and 400 diffraction peaks characterizes the state of the system in the irradiated layer from 0 to 6 μm (this layer is hereinafter referred to as a full layer).

When almost all of the hydrogen has left the matrix of the foil alloy after prolonged relaxation (8200 h), the phases for which a_{hkl} exceeds the lattice spacing of pure palladium ($a_{\text{Pd}} > 3.8903 \text{ \AA}$) are classified as a solid solutions of Pd–In, while the phases for which $a_{\text{Pd}} < 3.8903 \text{ \AA}$ are classified as phases of pure palladium with vacancies.

Table 1. The diffraction broadening and width of the curve of the CSR(hkl) distribution with respect to the concentration of In atoms for two states of the sample after hydrogenation and prolonged relaxation

hkl	$\beta_{h/2}$, deg	$\Delta a/a \times 10^{-3}$	$\beta_{h/2}$, deg	$\Delta a/a \times 10^{-3}$	$\beta_{h/2}$, deg	$\Delta a/a \times 10^{-3}$	$\beta_{h/2}$, deg	$\Delta a/a \times 10^{-3}$
	A side Hydrogenation I		B side Hydrogenation I		A side Hydrogenation II		B side Hydrogenation II	
111	0.075	1.83	0.017	0.41	0.133	3.25	0.108	2.66
200	0.079	1.65	0.040	0.88	0.268	5.51	0.258	5.31
220	0.059	0.78	0.035	0.46	0.267	3.87	0.186	4.83
311	0.095	0.97	0.030	0.31	0.469	4.83	0.477	2.46
222	0.039	0.37	0.040	0.36	0.311	2.93	0.150	1.41
400	0.099	0.68	0.079	0.55	0.832	5.76	0.622	4.29

During the saturation of the samples with hydrogen, a great number of vacancies enter the alloy matrix and this process induces the formation of defect complexes in the matrix [1, 2]. These can be planar defects of great size, whose specific volume differs from that of the matrix. In [2], the defects that have a specific volume that is greater than the alloy matrix are called D–M (defect–metal) complexes and those that have a smaller specific volume were called H–D–M–V (hydrogen–defect–metal–vacancy) complexes. The absolute value of the elastic stresses (σ) of the alloy matrix depends on the number of such complexes and their power. The value σ can have different signs: $\sigma > 0$ means that there are elastic compression stresses in the alloy matrix and $\sigma < 0$ means that there are tensile stresses. During degassing (during relaxation), the disintegration of the defect complexes, as well as the transformation of H–D–M–V complexes into D–M complexes can take place [2].

In [8] it was shown that the Reuss model of an elastically-stressed polycrystal accurately describes the experimental results on the determination of the lattice spacing for both deformed and hydrogenised palladium-based alloys. The values a_{hkl} , which are determined using the locations of diffraction peaks of different CSRs, meet the Royce formula:

$$a_{hkl} = a_0 + a_0 \sigma K_{hkl}, \tag{6}$$

where a_0 is the spacing of the undistorted cubic lattice; K_{hkl} is a value that depends on the elastic constants of the crystal and crystallographic direction; and σ is the value of elastic stresses.

The concentration of single vacancies in the sample is calculated similarly [6]:

$$n_{\text{vac}} = \frac{3 \cdot \Delta a}{a \cdot 0.22}, \tag{7}$$

where Δa is the decrease of the lattice spacing due to the entry of vacancies into the alloy matrix and (0.22) is the change in the volume upon forming a single vacancy.

3. EXPERIMENTAL RESULTS

3.1. The State of the Foil after the First Hydrogenation and Prolonged Relaxation

Figure 1 shows diffractograms for two orders of reflections from CSR(100) and CSR(111) for both foil sides after the first hydrogenation and relaxation (8200 h). It can be seen that in a number of cases the diffraction peaks are not described by one curve and there are differences in the shapes of curves of one CSR depending on the side on which hydrogen enters the foil.

The calculations show that for the phase characterized by the highest-intensity peak (which is hereinafter referred to as the master phase), the lattice spacings and elastic stresses are as follows: for the A side, $a_0 = (3.9078 \pm 0.0004) \text{ \AA}$ and $\sigma = (6 \pm 2) \text{ kg/mm}^2$; for the B side, $a_0 = (3.9070 \pm 0.0004) \text{ \AA}$ and $\sigma = 0 \text{ kg/mm}^2$. Using the Vegard dependence [11], the concentration of In atoms is determined for the master phase: $C_{\text{In}} = (5.3 \pm 0.1) \text{ at } \%$ for the A side and $(5.1 \pm 0.1) \text{ at } \%$ for the B side. Thus, the conclusion can be made that the concentration of In atoms for both sides of the foil for the master phase after relaxation (8200 h) was proven to be close to the concentration before the hydrogenous action on the sample. The positive value of σ for the A side indicates that defect complexes involving both hydrogen atoms and vacancies (H–D–M–V complexes) remain in the matrix of the master phase, while there are no elastic stresses in the initial state of the foil (see the control sample). For the B side, $\sigma = 0$ means that there are H–D–M–V complexes in the alloy matrix, but their specific volume equals to the specific volume of the matrix due to the large number of vacancies in the complexes.

The analysis of the diffractograms shows that the use of the alloy foil as a filter for obtaining hydrogen due to nontrivial relaxation processes that occurred through the year results in the broadening of diffraction peaks of the master phase, regardless of the direction of hydrogen entering the foil (see Table 1). The comparison of the broadening allows one to make the

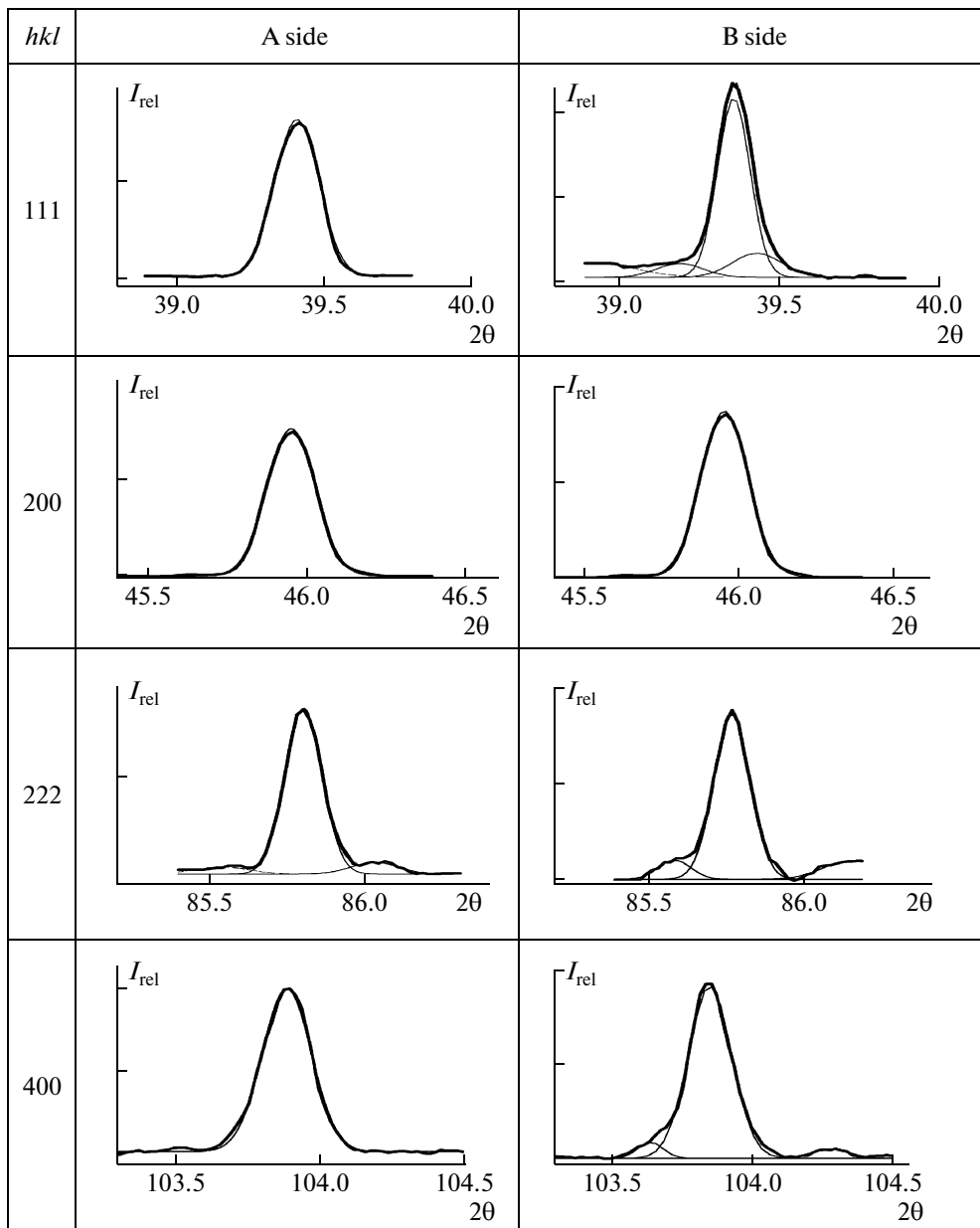


Fig. 1. Diffractograms (and their processing) of the alloy foil after the first hydrogenation and prolonged relaxation for two orders of reflections of CSR(100) and CSR(111).

conclusion that the values $\beta_{h/2}$ of the master phase for the B side are much lower than those for the A side, especially for the first orders of reflection. Since condition (5) must hold in the case of the second-class defects [12] in the alloy matrix and the calculations show that this inequality does not hold for the studied foil state, this indicates that the broadening of the peaks is due to the fact that the distribution of CSR with respect to the concentration of In atoms in the foil is not described by the δ -function. It will be greater, the wider the distribution of CSR(*hkl*) is with respect to the concentration of In atoms, which is

described by the function $\varphi(C_{\text{at \% In}})$ that is characterized by the value $\frac{\Delta a}{a}$. It can be seen from Table 1 that

the value $\frac{\Delta a}{a}$ for the A side considerably decreases

with the depth of the foil layer from which a certain diffraction peak is registered, with the dependence on the depth being much weaker for the B side. Moreover,

for the near-surface layer, the value $\frac{\Delta a}{a}$ for the B side is considerably lower than for the A side. The calcula-

Table 2. Percentage of additional phases and the concentration of In atoms/vacancies after hydrogenation and prolonged relaxation

<i>hkl</i>	$C \pm 0.2$, at % In	Phase percentage, (± 0.3)%	$C \pm 0.2$, at % In	Phase percentage, (± 0.3)%	$C \pm 0.2$, at % In	Phase percentage, (± 0.3)%	$C \pm 0.2$, at % In	Phase percentage, (± 0.3)%
	A side Hydrogenation I		A side Hydrogenation II		B side Hydrogenation I		B side Hydrogenation II	
111			25.8 13.6 0, $C_v = 0.5\%$	3.7 4.2 2.5	18.2 9.7 0	12.0 10.8 13.4	20.0 13.5	9.7 2.3
200			0, $C_v = 6.3\%$	1.4				
220			12.4	1.6			13.6 9.0 1.8 0, $C_v = 0.6\%$	2.5 5.6 18.1 2.1
311	8.7	4.0	4.7 8.0 0, $C_v = 0.6\%$	17 2.0 2.7	6.7 7.7	1.6 1.7	18.1 14.5 0, $C_v = 0.9\%$ 0, $C_v = 3.9\%$ 0, $C_v = 9.8\%$	2.3 1.4 7.2 1.6 1.4
222	8.3 2.8	5.5 7.7	17.1 14.3 0.9 0, $C_v = 4.2\%$	2.2 3.2 11.2 2.5	7.1 0.7	8.2 13.6	15.8 12.9 11.4 8.7 2.5 0.4	1.3 1.5 2.3 8.7 20.7 2.9
400			2.4 0, $C_v = 1.4\%$ 0, $C_v = 5.3\%$	8.0 4.2 3.9	6.7 1.5	5.0 3.5	13.8 2.4 0.3 0, $C_v = 3.5\%$	2.2 10.0 12.5 4.8

tions also show that for the A side the peak of the first order of reflection of CSR(100) for the master phase is narrower by 13% than the peak of the second order, while the diffraction peak of 111 is wider by 25% than that of 222. Moreover, the 111 diffraction peak for the A side is 4.4 times wider than that for the B side and for the first orders of reflection of CSR(100) the broadening of the corresponding peaks of the sides differ by 2 times.

Figure 1 shows that there are extra peaks with small intensities on the diffractograms of this state of the sample; their number is greater for the second orders of reflection. Table 2 gives the concentrations of In atoms (or vacancies) that are contained in the additional phases (as well as their percentage) corresponding to the extra peaks on the diffractograms.

It can be seen that the diffraction peaks that correspond to the additional phases occur in CSR(311) and CSR(111) from both sides of the foil, while there are

no such peaks among CSR(100) in the near-surface layer (0–3 μm), but they occur in the full layer of the B side. In CSR(100) of the B side, the phase in which the concentration of In atoms is far lower than in the master phase (1.5 at %) and the phase in which the concentration is somewhat greater (6.7 at %) occur for the second order of reflection. Moreover, the peak that corresponds to the master phase of the sample from the B side is narrower by 25% than that for the A side where there are no additional phases. The same regularity holds in the near-surface layer among CSR(111) of the B side. Phases with 17.6 at % In and 9.3 at % In at percentages of 12 and 10.8%, respectively, were found; as well, a phase of pure palladium with 2.4% was detected. It was also found that the diffraction peak that corresponds to the master phase for the B side is narrower (0.017°) than that for the A side (0.075°).

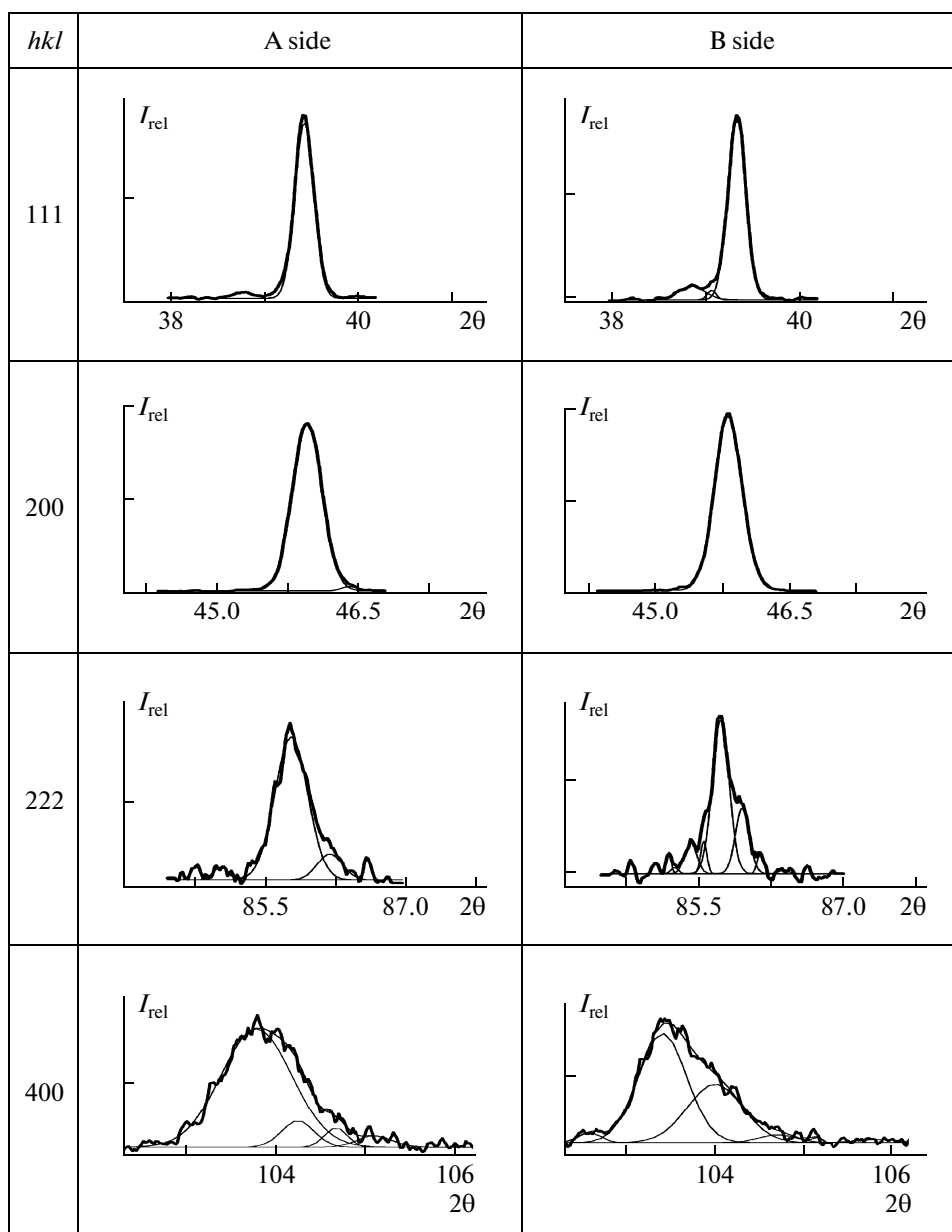


Fig. 2. Diffractograms (and their processing) of the alloy foil after the second hydrogenation and prolonged relaxation for two orders of reflections of CSR(100) and CSR(111).

Note that the number of additional phases with concentrations of In atoms that considerably differ from the average with respect to the layer, is greater from the B side (9 versus 3). The average percentage of the observable additional phases among CSR(111) for the A side is about 13%, while for the B side it is 23%.

The above issues allows one to make the conclusion that, despite the prolonged relaxation of the alloy after the first hydrogenation, the initial state of the foil was not restored completely; this is indicated by both the smearing of the diffraction peaks of the master phase and the weak-intensity peaks on the diffractograms,

which characterize the occurrence of additional phases (in which the concentration of In atoms considerably differs from that for the master phase) in the foil.

3.2. The State of the Foil after the Second Hydrogenation and Prolonged Relaxation

The diffraction patterns of the sample for the state that corresponds to relaxation (during 8200 h) after electrolytic hydrogenation are presented in Fig. 2. It can be seen that a considerable change in the shape of diffraction lines takes place as compared to the state that corresponds to the same relaxation period when

using the foil as a membrane. These changes especially affect the full scattering layer. For the latter, the increase in the number of components of diffraction peaks (which suggests the increased multiphase nature of the system) as well as the asymmetry of lines to the right of the main peak (which indicates the origination of vacancy-enriched phases in the sample) occur.

For the master phase of the saturation side, $a_0 = (3.9090 \pm 0.0004) \text{ \AA}$ and $\sigma = 0 \text{ kg/mm}^2$; for the opposite side, $a_0 = (3.9076 \pm 0.0004) \text{ \AA}$ and $\sigma = (-9 \pm 2) \text{ kg/mm}^2$. With the value of elastic stresses from the B side being zero before electrolytic hydrogenation, the negative σ indicates that the power of defect complexes is sharply increased in the alloy matrix from this side and that the complexes are D–M complexes. Most likely, the zero elastic stresses from the A side suggest that the defect complexes of the side still contain hydrogen (they correspond to H–D–M–V complexes), but their specific volume equals to the specific volume of the matrix due to the fact that there are a great number of vacancies in the complexes. Thus, one can conclude that the transformation of the defect complexes occurs faster for the B side than for the A side.

According to the Vegard dependence, the concentration of In atoms for the master phase of the A side is $C_{\text{In}} = (5.7 \pm 0.1) \text{ at } \%$, while for the master phase of the B side it is $C_{\text{In}} = (5.2 \pm 0.1) \text{ at } \%$. The comparison with the state prior to electrolytic hydrogenation shows an increase in the concentration of In atoms by 0.4 at % for the saturation side and by 0.1 at % for the opposite side.

Figure 2 and Table 2 show that the greatest number of additional phases occur for CSR(111) for both sides of the foil, while in the near-surface layer there are no additional phases from the A side after the first saturation and prolonged relaxation, although the diffraction lines are rather wide. After the second saturation, the percentage of additional phases in the near-surface layer (0–3 μm) of the A side is 10%, while it increased from 12.5 to 20% in the full layer. The same picture is observed for CSR(100) of the A side: the percentage of additional phases increased from 0 to 1.4% in the near-surface layer and from 0 to 16% in the full layer.

Note that electrolytic hydrogenation and prolonged relaxation result in the origination of the additional vacancy-enriched phases in the alloy matrix, which are not observed after the first hydrogenation. It can be seen from Table 2 that the percentage of the Pd–Vac phases among CSR(111) of the A side is the same throughout the scattering layer (about 8%); however, in the near-surface layer, the concentration of vacancies in the phases is eight times lower than in the full layer. Among CSR(100) in the near-surface layer, the Pd–Vac phase occupies 1.4% of the overall volume, but the concentration of vacancies in it is large (6.3%); in the full layer, the Pd–Vac phases make up 8%, while the average concentration of vacancies in them is close to 3.3%. Therefore, the conclusion can

be made that the number of vacancies that are contained in the additional coexisting phases that result from the hydrogenation and prolonged relaxation of the foil after electrolytic hydrogenation increase with the increasing depth of the foil layer.

The physical broadening of the diffraction peaks that correspond to the master phase was also found to be increased considerably (as compared to the state prior to electrolytic hydrogenation), i.e., the value $\frac{\Delta a}{a}$ increased considerably (see Table 1). The increase of the physical broadening of the main diffraction peaks was from 1.5 (CSR(111)) to 6 (CSR(100)) times, which is indicative of a wider distribution of CSR(111) and CSR(100) with respect to the concentration of In atoms as compared to the state prior to electrolytic hydrogenation. Moreover, for this state, the diffraction peaks of CSR(100) are 2.5 times wider than those of CSR(111) for both sides of the foil, with the width of the function of the CSR distribution with respect to the concentration of the alloying component being almost the same throughout the irradiated layer for different orders of reflection.

4. CONCLUSIONS

The analysis of the experimental data for both methods of hydrogenation and prolonged relaxation allows one to make the following conclusions.

For the first time, phases of pure palladium enriched with a great number of vacancies whose concentration increased with increasing depth of the foil layer were detected in an alloy foil as a result of prolonged relaxation after electrolytic saturation. A great number of such phases were detected for CSR(100).

It was found that after hydrogenation during the prolonged relaxation new phases were formed via broadening of the distribution of CSRs with respect to the concentration of In atoms of the master phase. Upon reaching a certain width of the distribution, additional diffraction peaks were formed along the edges of the diffraction peak of the master phase, which resulted in a decreasing width of the CSR distribution curve of the master phase.

The greatest number of additional phases were observed for the second orders of CSR(111) (in deeper layers of the foil), regardless of the side and hydrogenation method.

The use of Pd–5.3 at % In–0.5 at % Ru alloy foil as a membrane for obtaining high-purity hydrogen, despite its use at a high temperature (300°C) and further prolonged air storage resulted in considerable stratification of a homogeneous sample into coexisting phases in which the percentage and concentration of indium were considerably different for CSRs of different orientations. This fact is indicative of a possible change of the strength and hydrogen-permeability

characteristics of a membrane made from a foil of this composition.

The entire set of experimental data indicates the nontrivial evolution of phase-structure transformations in the foil after hydrogenation. A 1 year period of relaxation (regardless of the hydrogenation method) did not result in the restoration of the initial state of the foil. During the relaxation, the redistribution of In atoms with respect to the depth of the foil occurred via diffusion—cooperative travel of alloying components (hydrogen, vacancies, and metal atoms) between the matrix and the defect complexes.

ACKNOWLEDGMENTS

We thank RAS Corr. Fellow G.S. Burkhanov for the samples he provided.

REFERENCES

1. A. I. Olemskoi and A. A. Katsnel'son, *Sinergetics of Condensed Medium* (Moscow: URSS, 2003) [in Russian].
2. V. M. Avdyukhina, A. A. Katsnel'son, and G. P. Revkevich, *Poverkhnost. X-ray, Synkhr. Neitr. Issl.*, No. 2, 30 (1999).
3. V. M. Avdyukhina, A. A. Anishchenko, A. A. Katsnel'son, and G. P. Revkevich, *Phys. Solid State* **46**, 265 (2004).
4. G. S. Burkhanov, N. B. Gorina, N. B. Kolchugina, and N. R. Roshan, *Ros. Khim. Zhurnal (Zh. Ros. Khim. Ob-Va Im. D.I. Mendeleeva)*, No. 4, 36 (2006).
5. G. S. Burkhanov, N. B. Gorina, N. B. Kol'chugina, et al., *Proc. 2nd Int. Symp. on Hydrogen Energetics* (Moscow, 2007).
6. V. M. Avdyukhina, O. V. Akimova, I. S. Levin, and G. P. Revkevich, *Russ. Metall. (Metally)*, No. 7, 646 (2011).
7. V. M. Avdyukhina, O. V. Akimova, I. S. Levin, and G. P. Revkevich, *Mos. Univ. Phys. Bull.* **66**, 33 (2011).
8. Y. Fukai and N. Okuma, *Phys. Rev. Lett.* **73**, 1640 (1994).
9. N. I. Lyakishev, *State Diagrams of Binary Metallic Systems* (Moscow: Mashinostroenie, 1999) [in Russian].
10. V. I. Iveronova and G. P. Revkevich, *X-ray Dispersion Theory* (Moscow, 1978) [in Russian].
11. M. L. Wise, G. P. Farr, and I. R. Harris, *J. Less. Common. Met.* **41**, 115 (1975).
12. M. A. Krivoglaz, *X-ray and Neutron Diffraction in Non-ideal Crystals* (Kiev, 1983) [in Russian].

Translated by Yu. Kornienko